

# Voltage-controlled magnetic anisotropy in antiferromagnetic MgO-capped MnPt films

P.-H. Chang,<sup>1,\*</sup> W. Fang,<sup>1</sup> T. Ozaki,<sup>2</sup> and K. D. Belashchenko<sup>1</sup>

<sup>1</sup>*Department of Physics and Astronomy and Nebraska Center for Materials and Nanoscience, University of Nebraska-Lincoln, Lincoln, Nebraska 68588, USA*

<sup>2</sup>*Institute for Solid State Physics, The University of Tokyo, 5-1-5 Kashiwanoha, Kashiwa, Chiba 277-8581, Japan*

The magnetic anisotropy in MgO-capped MnPt films and its voltage control are studied using first-principles calculations. Sharp variation of the magnetic anisotropy with film thickness, especially in the Pt-terminated film, suggests that it may be widely tuned by adjusting the film thickness. In thick films the linear voltage control coefficient is 0.17 and  $-0.07$  pJ/Vm for Pt-terminated and Mn-terminated interfaces, respectively, which is comparable to the Fe|MgO interface. The combination of a widely tunable magnetic anisotropy energy and a sizeable voltage-control coefficient suggest that MgO-capped MnPt films can serve as a versatile platform for magnetic memory and antiferromagnonic applications.

Interfacial magnetic anisotropy can be tuned by applying an electric field through an electrolyte [1] or, more practically, across a tunnel junction [2–4]. This technique, called voltage-controlled magnetic anisotropy (VCMA), can be used to facilitate switching in memory devices [5–9], control the motion of domain walls [10, 11], and excite and manipulate spin waves in magnonic devices [12–22].

The vast majority of VCMA studies have focused on ferromagnetic materials. However, there is a lot of interest in incorporating antiferromagnets (AFM) in spintronic devices [23–25], harnessing their ultrafast dynamics and insensitivity to magnetic fields for improved switching speed and scalability. Piezoelectric strain control has emerged as an important way to tune the properties of an AFM material in a device [26–28], but interfacial VCMA based on electrostatic screening can also serve as a tuning mechanism in devices utilizing metallic AFM materials [27, 29–31] and even enable coherent AFM domain switching by picosecond voltage pulses [32].

It is natural to look for AFM materials with relatively small and tunable bulk magnetic anisotropy energy (MAE), which would allow the MAE of a thin film to be engineered to the desired range. One such material is L1<sub>0</sub>-ordered tetragonal MnPt, which can be tuned across spin reorientation transitions (between easy-axis and easy-plane) by off-stoichiometry, temperature variation, and epitaxial strain [33–36]. It has been shown that MnPt pillars can be reversibly switched between different magnetic states by electric currents [37], and it is compatible with silicon technology [38]. In this paper, we study MAE and VCMA in MgO|MnPt|MgO films in a wide range of MnPt thicknesses, with both Mn- and Pt-terminated interfaces. Based on our results, we propose that the film with a Pt-terminated MnPt|MgO interface can serve as a versatile, tunable platform for antiferromagnonic applications.

We consider L1<sub>0</sub>-MnPt films capped by 3 monolayers (ML) of MgO on each side in a periodic setup with 2 nm of vacuum separating the two MgO layers. The MnPt|MgO interfaces are either both Pt-terminated or both Mn-terminated. This structural setup is shown in Fig. 1. We impose the bulk magnetic structure of MnPt, with staggered magnetic moments in

the (001) planes and ferromagnetic spin alignment along the [001] axis. The structure is optimized using the projector-augmented wave (PAW) method [39] implemented in the Vienna Ab Initio Simulation Package (VASP) [40]. The experimental [33] bulk value of  $4.00 \text{ \AA}$  is used for the in-plane lattice constant and kept fixed in all calculations. For films with up to 19 ML of MnPt, the atomic coordinates along the out-of-plane axis are relaxed at zero electric field until the forces are less than  $1 \text{ meV/\AA}$ ; the in-plane coordinates are fixed by symmetry. Thicker films are obtained by inserting additional MnPt layers in the middle with the bulk interlayer spacing.

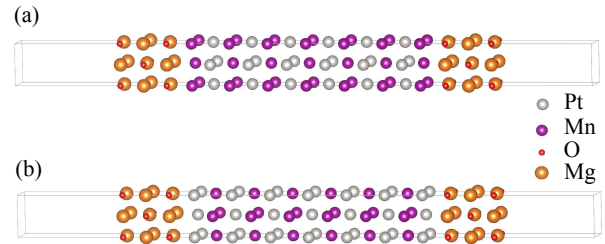


FIG. 1. Computational setup for (a) Mn-terminated or (b) Pt-terminated MnPt films capped with MgO.

Magnetic anisotropy calculations were carried out using the OpenMX code with a pseudo-atomic orbital basis [41–43], using the generalized gradient approximation (GGA) [44] for exchange and correlation. The charge and spin densities were obtained using a self-consistent calculation without spin-orbit coupling (SOC) and kept fixed in subsequent MAE calculations. At zero field, the MAE of a film was determined as the difference in the total band energy for the configurations with the magnetization aligned in-plane and out-of-plane.

The electric field was introduced by inserting an electrostatic dipole layer in the middle of the vacuum layer. This setup makes the electric field point outward on one MgO/MnPt interface and inward on the other, and the linear effect of the field on the total MAE of the film is zero. Therefore, the analysis of VCMA requires the contributions of the two interfaces to be separated. To this end, we calculate the site-resolved grand canonical potential  $\Omega_i = E_i - E_F N_i$ , where  $E_i$  and  $N_i$  are the site-resolved band energy and Mullikan pop-

\* Present address: Department of Physics, The University of Texas at El Paso, 500 W. University Ave., El Paso, Texas 79968, USA

ulation [45]:

$$E_i = \text{Tr} \sum_j \hat{\rho}_{ij} \hat{H}_{ji}, \quad (1)$$

$$N_i = \text{Tr} \sum_j \hat{S}_{ij} \hat{\rho}_{ji}. \quad (2)$$

Here  $i, j$  are site indices,  $\hat{\rho}_{ij}$  is density matrix,  $\hat{H}_{ij}$  the Kohn-Sham Hamiltonian in the real-space representation, and  $\hat{S}_{ij}$  the overlap matrix; the trace is taken over spin and orbital indices. The site-resolved MAE can then be found as the difference between the site-resolved grand potentials corresponding to the in-plane and out-of-plane orientations of the magnetic moments:  $K_i = \Omega_i(\parallel) - \Omega_i(\perp)$ . This is done as a function of the electric field, and the anisotropy of one interface  $K_{int}$  is found by summing up  $K_i$  for the sites that are closer to the given interface than the other. Note that Eqs. (1)-(2) partition off-diagonal terms equally between the two sites, which is not invariant under a unitary transformation. However, because the Hamiltonian is short-ranged in the OpenMX basis set, this ambiguity is immaterial as long as the MnPt layer is not too thin.

Figure 2 shows the total MAE  $K$  of MgO-capped MnPt films as a function of MnPt thickness  $d$  at zero electric field. Three types of films are considered: (a) both interfaces terminated by Mn, (b) both interfaces terminated by Pt, and (c) one interface of each kind. As the thickness of the film is increased, the  $K(d)$  dependence should eventually approach a straight line with a slope equal to the bulk MAE. We see that this asymptotic behavior is only observed in rather thick films, especially if the interfaces are Pt-terminated. The asymptotic slope is close to zero, because the bulk MAE in stoichiometric MnPt is very small [33, 35]. Slowly decaying oscillations persist up to the largest thicknesses and are likely due to quantum size effects [46–48]. These oscillations may be damped by interface roughness and disorder in an actual sample. As it should, the MAE of a film with one interface of each kind (black line in Fig. 2) asymptotically approaches the average of the films with both interfaces terminated by Pt or Mn, but this also happens at rather large thicknesses.

The y-intercept of the asymptotic  $K(d)$  dependence is the effective interfacial MAE of a thick film. This interfacial MAE appears to be small for Mn-terminated films, but it is large and negative for Pt-terminated films. Small MAE in bulk stoichiometric MnPt is a result of a cancellation of large contributions of opposite sign [36]. The large interfacial MAE in Pt-terminated films suggests that this delicate cancellation is broken at this interface, while it is preserved at the Mn-terminated interface.

For thicknesses up to 10-15 ML, Fig. 2 shows sharp variations of MAE. In this region, the two interfaces strongly interact, and it makes no sense to talk about separate bulk and interfacial contributions. In Mn-terminated films, MAE shows large oscillations, which appear to have the same character as the decaying oscillations at larger thicknesses. However, in Pt-terminated films the MAE declines monotonically from about 4 to  $-3$  mJ/m<sup>2</sup> as the MnPt thickness increases from 5 to 15 ML. To understand this decline, we compare the partial

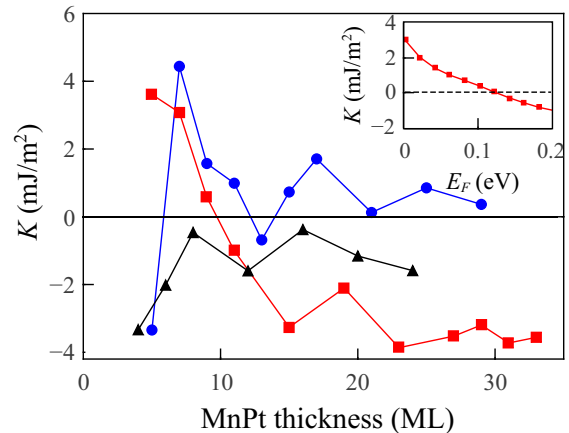


FIG. 2. Thickness dependence of the total MAE of MgO-capped MnPt films with two Mn-terminated interfaces (blue circles), two Pt-terminated (red squares), or one interface of each kind (black triangles). Inset: MAE of the 7-ML-thick Pt-terminated film as a function of the Fermi energy (rigid-band calculation).

density of states (DOS) on the four MLs of MnPt near the Pt-terminated interface for films with 7, 15 and 23 ML or MnPt. As seen in Fig. 3, there is a notable downward shift of about 0.2 eV, between 7 and 15 ML, in the position of the DOS peak right below the Fermi energy. It is well known that the MAE of a metallic system tends to be sensitive to the occupation of the electronic states near the Fermi energy. The inset in Fig. 2 shows the MAE in a 7-ML Pt-terminated film as a function of the Fermi level, calculated in the rigid-band approximation. Raising the Fermi level by 0.2 eV, which corresponds to the band shift between 7 and 15-ML films, reduces the MAE from 3 to  $-1$  mJ/m<sup>2</sup>. This is similar to the decline observed in the thickness dependence seen in Fig. 2.

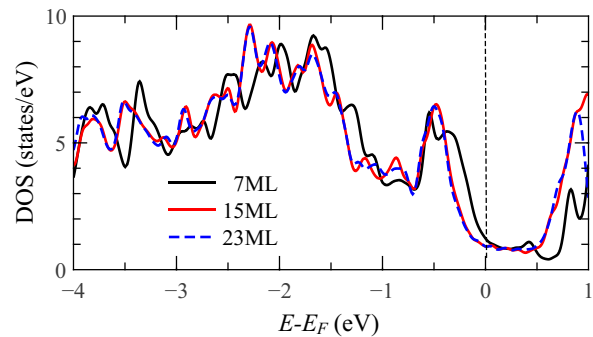


FIG. 3. Comparison of the contributions from the first four layers to total DOS among the Pt-terminated films of thicknesses 7, 15 and 23 ML. The dashed line indicates the Fermi level.

Now we turn to VCMA. It is customary to define this response with respect to the electric field inside the insulator, which is directly related to gate voltage. Within macroscopic electromagnetism, the field  $E_{\text{MgO}}$  in MgO in our computational setup is reduced by the relative dielectric permittivity

$\epsilon_r$  compared to the field  $E_{vac}$  in the vacuum layer. The value of  $\epsilon_r$  is not well described in the calculations due to the inaccuracies of the density-functional theory and the exclusion of field-induced ionic displacements. On the other hand, it is reasonable to expect that VCMA is largely controlled by the density of the screening charge accumulated at the interface [2], which is related to the electric induction in MgO. The latter is equal to  $\epsilon_0 E_{vac}$  and does not depend on  $\epsilon_r$ . Therefore, following Ref. 49, we estimate the electric field in the MgO layer as  $E_{MgO} = E_{vac}/\epsilon_r$ , where  $\epsilon_r = 9.5$  is the experimental value for MgO. The linear VCMA coefficient is then defined as  $\beta = \epsilon_r dK_{int}/dE_{vac}$ , where  $K_{int}$  is the anisotropy of one interface obtained as explained after Eqs. (1)-(2).

The exterior normal to the metallic surface was taken as the positive direction of the electric field. Rather dense  $k$ -point meshes were needed to converge the linear VCMA coefficient  $\beta$ :  $65 \times 65$  for Pt-terminated and  $35 \times 35$  for Mn-terminated films, respectively.

Figure 4 shows the change in the site-resolved MAE ( $\Delta K_i$ ) induced in 19-ML MgO-capped MnPt films by  $E_{vac} = 1.0$  V/nm. The response in the Pt-terminated film is notably non-linear in this strong field, which is reflected in deviations from antisymmetry with respect to the middle of the film. We also see that the response has opposite signs for the two interface terminations. The induced anisotropy  $\Delta K_i$  is localized within 3 or 4 layers of metal near the interface, which include, for both terminations, two Mn layers closest to the surface and the intervening Pt layers. The MgO layer near the interface also contributes to VCMA. As noted above, the assignment of MAE to atomic sites has an inherent ambiguity on the short length scales corresponding to the range of the atomic orbitals.

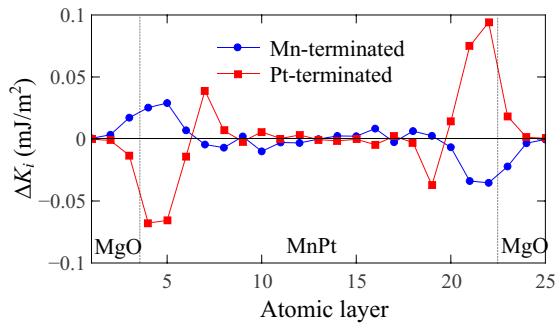


FIG. 4. Change in the site-resolved MAE induced by  $E_{vac} = 1.0$  V/nm in 19-ML films with two types of interface termination.

Figure 5(a) shows the change in the induced interfacial MAE  $\Delta K_{int}$  as a function of the estimated electric field in MgO for 15-ML Mn-terminated and 23-ML Pt-terminated films, and the linear VCMA coefficient  $\beta$  is plotted in Fig. 5(b) as a function of the film thickness. The large thicknesses in panel (a) were chosen so that the  $\beta$  coefficient has approached its asymptotic value for the given interface termination.

The  $\beta$  coefficient at the Pt-terminated MnPt/MgO interface (0.17 pJ/Vm in thick films) is similar to the *ab initio* results for the Fe/MgO interface [49, 50]. Mn-terminated interfaces have a smaller  $\beta$  of an opposite sign ( $-0.06$  pJ/Vm in thick films).

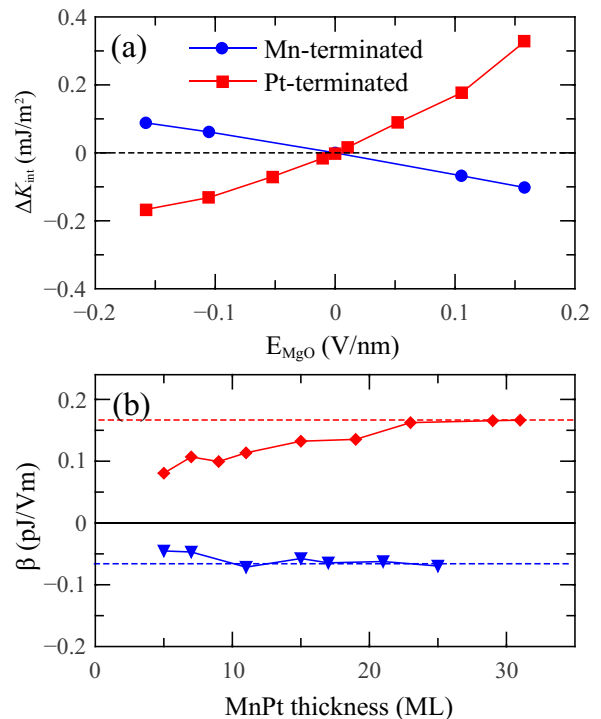


FIG. 5. (a) Induced interfacial anisotropy  $\Delta K_{int}$  as a function of the estimated electric field  $E_{MgO}$  for 15-ML-thick Mn-terminated and 23-ML-thick Pt-terminated films. (b) Linear VCMA coefficient  $\beta$  as a function of MnPt thickness.

Larger VCMA for the Pt-terminated surface, compared to Mn-terminated, was also found theoretically and experimentally for FePt [51, 52].

Our results suggest that a thin MgO-capped MnPt film can serve as a versatile platform for antiferromagnonic applications. Both Pt-terminated and Mn-terminated MnPt/MgO interfaces are predicted to have a sizeable linear VCMA coefficient (0.05–0.15 pJ/Vm) comparable to the ferromagnetic Fe/MgO interface. A Pt-terminated film appears to be particularly attractive due to its sharp monotonic decline in the total MAE as a function of thickness, from nearly 4 mJ/m<sup>2</sup> to nearly  $-4$  mJ/m<sup>2</sup>, in the range between 5 and 15 ML (see Fig. 2). This property may help tune the MAE of the Pt-terminated film to any desired value in this range by adjusting its thickness. Fig. 2 suggests that such tuning may be possible even if the termination of the film is not strictly controlled. On the other hand, the MnPt compound has a high Néel temperature of almost 1000 K [33], which is favorable for applications. Large sensitivity of the bulk MAE in MnPt to non-stoichiometry, temperature, and strain [33–36] provides additional options for tuning the MAE of a film for optimal device performance. Voltage control of anisotropy through local gates can be used to implement spin wave generation, logic, and detection by analogy with ferromagnets [19–22], and it may also enable ultrafast switching of AFM order for memory applications [32].

## ACKNOWLEDGMENTS

We thank Ilya Krivorotov, Vasyl Tyberkevich, and Andrei Slavin for useful discussions. This work was supported by the Nanoelectronics Research Corporation (NERC), a wholly-owned subsidiary of the Semiconductor Research Corporation (SRC), through the Center for Nanoferroic De-

vices (CNFD), a SRC-NRI (Nanoelectronics Research Initiative) Center (Task ID 2398.003), and by the National Science Foundation through the Nebraska MRSEC (Grant No. DMR-1420645) and Grant No. DMR-1609776. Calculations were performed utilizing the Holland Computing Center of the University of Nebraska, which receives support from the Nebraska Research Initiative.

- 
- [1] M. Weisheit, S. Fähler, A. Marty, Y. Souche, C. Poinsignon, and D. Givord, *Science* **315**, 349 (2007).
- [2] C.-G. Duan, J. P. Velev, R. F. Sabirianov, Z. Zhu, J. Chu, S. S. Jaswal, and E. Y. Tsymlal, *Phys. Rev. Lett.* **101**, 137201 (2008).
- [3] M. Endo, S. Kanai, S. Ikeda, F. Matsukura, and H. Ohno, *Appl. Phys. Lett.* **96**, 212503 (2010).
- [4] P. Khalili Amiri and K. L. Wang, *SPIN* **02**, 1240002 (2012).
- [5] R. Dorrance, J. G. Alzate, S. S. Cherepov, P. Upadhyaya, I. N. Krivorotov, J. A. Katine, J. Langer, K. L. Wang, P. K. Amiri, and D. Marković, *IEEE Electron Device Lett.* **34**, 753 (2013).
- [6] Y. Shiota, T. Nozaki, F. Bonell, S. Murakami, T. Shinjo, and Y. Suzuki, *Nat. Mater.* **11**, 39 (2011).
- [7] W.-G. Wang, M. Li, S. Hageman, and C.-L. Chien, *Nat. Mater.* **11**, 64 (2011).
- [8] T. Seki, M. Kohda, J. Nitta, and K. Takanashi, *Appl. Phys. Lett.* **98**, 212505 (2011).
- [9] E. Grimaldi, V. Krizakova, G. Sala, F. Yasin, S. Couet, G. Sankar Kar, K. Garello, and P. Gambardella, *Nat. Nanotechnol.* **15**, 111+ (2020).
- [10] U. Bauer, S. Emori, and G. S. D. Beach, *Appl. Phys. Lett.* **101**, 172403 (2012).
- [11] A. Bernand-Mantel, L. Herrera-Diez, L. Ranno, S. Pizzini, J. Vogel, D. Givord, S. Auffret, O. Boulle, I. M. Miron, and G. Gaudin, *Appl. Phys. Lett.* **102**, 122406 (2013).
- [12] T. Brächer, P. Pirro, F. Heussner, A. A. Serga, and B. Hillebrands, *Applied Physics Letters* **104**, 092418 (2014).
- [13] R. Verba, V. Tiberkevich, I. Krivorotov, and A. Slavin, *Phys. Rev. Applied* **10**, 044006 (2014).
- [14] A. Capua, C. Rettner, and S. S. P. Parkin, *Phys. Rev. Lett.* **116**, 047204 (2016).
- [15] R. Verba, M. Carpentieri, G. Finocchio, V. Tiberkevich, and A. Slavin, *Scientific Reports* **6**, 25018 (2016).
- [16] Y.-J. Chen, H. K. Lee, R. Verba, J. A. Katine, I. Barsukov, V. Tiberkevich, J. Q. Xiao, A. N. Slavin, and I. N. Krivorotov, *Nano Lett.* **17**, 572 (2017).
- [17] Q. Wang, A. V. Chumak, L. Jin, H. Zhang, B. Hillebrands, and Z. Zhong, *Phys. Rev. B* **95**, 134433 (2017).
- [18] B. Rana, Y. Fukuma, K. Miura, H. Takahashi, and Y. Otani, *Appl. Phys. Lett.* **111**, 052404 (2017).
- [19] R. Verba, M. Carpentieri, G. Finocchio, V. Tiberkevich, and A. Slavin, *Phys. Rev. Applied* **7**, 064023 (2017).
- [20] R. Verba, M. Carpentieri, G. Finocchio, V. Tiberkevich, and A. Slavin, *Appl. Phys. Lett.* **112**, 042402 (2018).
- [21] B. Rana and Y. Otani, *Phys. Rev. Applied* **9**, 014033 (2018).
- [22] B. Rana and Y. Otani, *Commun. Phys.* **2** (2019).
- [23] T. Jungwirth, X. Marti, P. Wadley, and J. Wunderlich, *Nature Nanotechnology* **11**, 231 (2016).
- [24] V. Baltz, A. Manchon, M. Tsoi, T. Moriyama, T. Ono, and Y. Tserkovnyak, *Rev. Mod. Phys.* **90**, 015005 (2018).
- [25] T. Jungwirth, J. Sinova, A. Manchon, X. Marti, J. Wunderlich, and C. Felser, *Nat. Phys.* **14**, 200 (2018).
- [26] Z. Liu, Z. Feng, H. Yan, X. Wang, X. Zhou, P. Qin, H. Guo, R. Yu, and C. Jiang, *Adv. Electron. Mater.* **5** (2019), 10.1002/aelm.201900176.
- [27] H. Yan, Z. Feng, P. Qin, X. Zhou, H. Guo, X. Wang, H. Chen, X. Zhang, H. Wu, C. Jiang, and Z. Liu, *Adv. Mater.* **32** (2020).
- [28] P. Popov, A. Safin, A. Kirilyuk, S. Nikitov, I. Lisenkov, V. Tyberkevich, and A. Slavin, *Phys. Rev. Applied* **13**, 044080 (2020).
- [29] Y. Wang, X. Zhou, C. Song, Y. Yan, S. Zhou, G. Wang, C. Chen, F. Zeng, and F. Pan, *Adv. Mater.* **27**, 3196 (2015).
- [30] G. Zheng, S.-H. Ke, M. Miao, J. Kim, R. Ramesh, and N. Kioussis, *Sci. Rep.* **7** (2017), 10.1038/s41598-017-05611-7.
- [31] Y. Su, M. Li, J. Zhang, J. Hong, and L. You, *Journal of Magnetism and Magnetic Materials* **505**, 166758 (2020).
- [32] V. Lopez-Dominguez, H. Almasi, and P. Khalili Amiri, *Phys. Rev. Applied* **11**, 024019 (2019).
- [33] E. Krén, G. Kádár, L. Pál, J. Sólyom, P. Szabó, and T. Tarnóczy, *Phys. Rev.* **171**, 574 (1968).
- [34] H. Hama, R. Motomura, T. Shinozaki, and Y. Tsunoda, *J. Phys. Condens. Matter* **19**, 176228 (2007).
- [35] Z. Lu, R. V. Chepulsii, and W. H. Butler, *Phys. Rev. B* **81**, 094437 (2010).
- [36] P.-H. Chang, I. A. Zhuravlev, and K. D. Belashchenko, *Phys. Rev. Materials* **2**, 044407 (2018).
- [37] J. Shi, V. Lopez-Dominguez, F. Garesci, C. Wang, H. Almasi, M. Grayson, G. Finocchio, and P. K. Amiri, *Nat. Electron.* **3**, 92 (2020).
- [38] E. Reiss and M. Meinert, *Nat. Electron.* **3**, 75 (2020).
- [39] P. E. Blöchl, *Phys. Rev. B* **50**, 17953 (1994).
- [40] G. Kresse and D. Joubert, *Phys. Rev. B* **59**, 1758 (1999).
- [41] T. Ozaki, *Phys. Rev. B* **67**, 155108 (2003).
- [42] T. Ozaki *et al.*, OpenMX 3.8, <http://www.openmx-square.org>.
- [43] K. Lejaeghere *et al.*, *Science* **351** (2016).
- [44] J. P. Perdew, K. Burke, and M. Ernzerhof, *Phys. Rev. Lett.* **78**, 1396 (1997).
- [45] R. Cuadrado and J. I. Cerdá, *Journal of Physics: Condensed Matter* **24**, 086005 (2012).
- [46] U. Bauer, M. Dabrowski, M. Przybylski, and J. Kirschner, *Phys. Rev. B* **84**, 144433 (2011).
- [47] M. Przybylski, M. Dabrowski, U. Bauer, M. Cinal, and J. Kirschner, *Journal of Applied Physics* **111**, 07C102 (2012).
- [48] L. Szunyogh, B. Újfalussy, C. Blaas, U. Pustogowa, C. Sommers, and P. Weinberger, *Phys. Rev. B* **56**, 14036 (1997).
- [49] J. Zhang, P. V. Lukashev, S. S. Jaswal, and E. Y. Tsymlal, *Phys. Rev. B* **96**, 014435 (2017).
- [50] F. Ibrahim, H. X. Yang, A. Hallal, B. Dieny, and M. Chshiev, *Phys. Rev. B* **93**, 014429 (2016).
- [51] M. Tsujikawa and T. Oda, *Phys. Rev. Lett.* **102**, 247203 (2009).
- [52] S. Miwa, M. Suzuki, M. Tsujikawa, K. Matsuda, T. Nozaki,

K. Tanaka, T. Tsukahara, K. Nawaoka, M. Goto, Y. Kotani, T. Ohkubo, F. Bonell, E. Tamura, K. Hono, T. Nakamura, M. Shirai, S. Yuasa, and Y. Suzuki, *Nat. Commun.* **8**, 15848 (2017).